XLIII CILAMCE
21-25, November, 2022
FOZ DO IGUAÇU – PR – BRAZIL

A numerical study of damage evaluation in jointed plain SHCC pavements using new damage evolution laws

Edmir J. Santos Júnior, Rafael Marques Lins, Francisco A. C. Monteiro, Sérgio Gustavo Ferreira Cordeiro

Laboratório de Modelagem Estrutural – LME, Instituto Tecnológico de Aeronáutica
Praça Marechal Eduardo Gomes,50, Vila das Acácias, 12.228-900, São José dos Campos/SP, Brasil
edmir.junior@ga.ita.br, facm@ita.br, cordeiro@ita.br

Abstract. It is well-known in the design of jointed plain cementitious pavements (JPCP) that the damage in the cementitious matrix due to stress near the dowel bars is a key factor that affects the service life of such structures. This study aimed to evaluate numerically the differences in the damage distribution in the near dowel bar region in JPCP considering alternative materials: strain-hardening cementitious composites (SHCC) in substitution to concrete and glass fiber reinforced polymer (GFRP) in substitution to the steel bar. The adopted constitutive model for the cementitious materials was the concrete damage plasticity. A new damage evolution law proposed by the authors in [13] was adopted. Such a law can be very effective in reproducing the SHCC behavior because both damage and plastic strain variables are involved with. Interactions between the cementitious matrix and the dowel bars were simulated by surface-to-surface contact type. The finite element models were validated by comparing available experimental load-displacement curves with the obtained numerical ones. The results for the damage distributions reveal that the use of such alternative materials has induced smaller damage values within a smaller damaged zone when compared with the model with conventional materials: standard concrete and steel bars. Consequently, smaller cracks in such zones will appear which will increase the structural life of the pavement.

Keywords: jointed plain SHCC pavements, load transfer, damage plasticity, damage evolution laws.

1 Introduction

The jointed plain cementitious pavement (JPCP) consists of cementitious slabs separated by joints and rested on one or more foundation layers. The existence of construction joints in this type of pavement is inevitable independently of the type of cementitious materials adopted. Construction joints (Fig. 1a) stand between slabs and occur when concrete is poured over already existing concrete [1]. The long-term performance of JPCP is directly related to the load transfer efficiency at the joints. In conventional concrete, aggregate interlock is a natural load transfer device and consists of the mechanical closure formed in the joints. In the construction joints, this mechanism is absent, making the use of dowel bars mandatory as a load transfer device between slabs [2]. The load transfer through the dowel bars occurs by transversal shear and/or bending moment. This mechanism generates a stress concentration in the vicinity of the bars (Fig. 1b), making it a critical zone for microcracking. This degradation impacts the performance and service life of such structures [3]. Researchers have been testing alternative geometric design, as well as alternative cementitious materials and dowel bars, in order to reduce the stress concentration. Wakdar et. al. [4] evaluated the influence of dowel diameter, spacing, and length parameters on the load transfer efficiency in joints. Kim and Hjelmstad [5] and Mackiewicz [3] analyzed the dowel looseness and its implication on the stress state on the concrete in the vicinity of the dowel. Sadegui and Hesami [6] and Shoukry et. al. [7] evaluated the friction between the dowel and the concrete pavement. Prabhu et. al. [8] and Al-Humeidawi and Mandal [9] evaluated the consequences of misalignment of the dowels in relation to the level of stress around the bars. Al-Humeidawi and Mandal [10] evaluated experimentally the vertical displacement of dowel bars comparing steel bars with glass fiber reinforced polymer (GFRP) bars.

Different types of cementitious materials can be applied to pavement structure. Strain-hardening cementitious composites (SHCC) belongs to the class of fiber reinforced concretes (fiber reinforced concrete-FRC), as it contains fibers in a cementitious matrix. Nevertheless, unlike conventional FRC, the SHCC represent a family of materials with the common characteristic of presenting a strain-hardening behavior, with a capacity to strain under tension typically beyond 4% [11]. For comparison, more recently a type of high-performance concrete was developed, the ultra-high-performance concrete (UHPC), which stands out for its high compressive strength (above 150 MPa), but with a tensile strain capacity of the order of 0.2% [12]. This mechanical behavior of the SHCC has motivated several researchers around the world to investigate its use in different types of structures, including pavements.

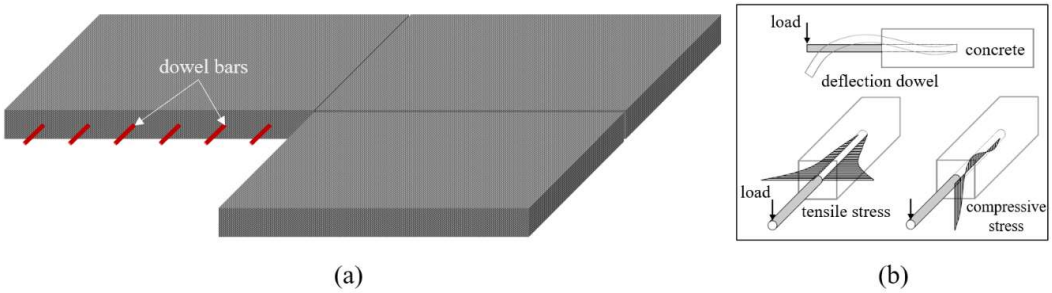

Figure 1. JPCP: (a) construction joints with dowel bars; (b) distribution of stress in a loaded dowel

In this study, a finite element model was developed in order to compare the damage of standard concrete and SHCC pavements in the vicinity of the dowel bars for two different types of dowel bars: steel and GFRP. A representative structure of a construction joint was modelled to evaluate the dowel bars behavior through a fully nonlinear (geometrical and material) finite element analysis. The constitutive model used for the cementitious materials was the concrete damage plasticity (CDP). The experimental results by Al-Humeidawi and Mandal [10] were used to validate the first stage finite element model regarding concrete with both steel and fiber reinforced dowel bars. Later, the damage evolution law proposed by the present authors in [13] and other CDP parameters calibrated for SHCC materials [14] were adopted to replace the conventional concrete by SHCC, in order to quantify the damaged region regarding such an alternative material.

2 Concrete damage plasticity constitutive model

The concrete damage plasticity (CDP) is a continuum constitutive model of scalar damage plasticity developed by Lubliner et. al. [15] and later modified by Lee and Fenves [16]. Cracks are represented macroscopically by stiffness degradation through a scalar damage variable. It assumes two main failure mechanisms for the concrete: tensile cracking and compression crushing. Thus, the scalar damage variable is defined as a function of scalar damage variables in tension and compression, plus the multiaxial stress state. The yield surface is controlled by the hardening variables $\tilde{\varepsilon}_t^p$ and $\tilde{\varepsilon}_c^p$, which corresponds to the equivalent tensile and compressive plastic strains, respectively, and are related to the failure mechanisms in tensile and compression. This model is capable of accurately predicting the response of different concrete structures under different types of loading [17] – [19].

2.1 Multiaxial damage plasticity model

Regarding small displacement gradient components, when compared to unity (infinitesimal strains), the strain tensor can be additively decomposed as:

$$\boldsymbol{\varepsilon} = \boldsymbol{\varepsilon}_e + \boldsymbol{\varepsilon}_p \tag{1}$$

where $\boldsymbol{\varepsilon}$ is the total strain tensor, $\boldsymbol{\varepsilon^e}$ is the elastic strain tensor and $\boldsymbol{\varepsilon^p}$ the plastic strain tensor. Assuming that the damage tensor can be fully characterized by a scalar damage D, the stress-strain relationship for general multiaxial case results:

$$\boldsymbol{\sigma} = (\boldsymbol{II} - \boldsymbol{D})\boldsymbol{C}_0 : (\boldsymbol{\varepsilon} - \boldsymbol{\varepsilon}_p) \tag{2}$$

$$\boldsymbol{\sigma} = (\boldsymbol{II} - D\boldsymbol{II})\boldsymbol{C}_0 : (\boldsymbol{\varepsilon} - \boldsymbol{\varepsilon}_p)$$

$$\boldsymbol{\sigma} = (1 - D)\boldsymbol{C}_0 : (\boldsymbol{\varepsilon} - \boldsymbol{\varepsilon}_p)$$

where $\boldsymbol{\sigma}$ is the Cauchy stress tensor, $\boldsymbol{C}_0$ is the elastic constitutive tensor, **D** is the damage tensor, **II** is the fourth order identity and D is a scalar damage variable. Despite the previous presented isotropic damage assumption, in cementitious materials, when one or more principal stresses changes from compression to tensile, the stiffness degradation mechanism becomes quite complex. This occurs due to what is observed in the microstructural behavior of the material (cracks originating from a principal tensile stress tends to close due to the change of the principal stress to compression). It is assumed that an isotropic damage model with a scalar damage variable D_t is capable of accurately representing the behavior of cementitious materials undergoing stress states with only tensile principal stresses. Analogous assumption is made, regarding a scalar damage variable D_c, when the cementitious material undergoes stress states with only compression principal stresses. For general multiaxial stress states, the concept of stiffness recovery, i.e., the crack closure reverts to an increase in the material stiffness, can be applied to relate the general scalar damage variable D with the tensile and compressive damage variables D_t, D_c and the stress state $\boldsymbol{\sigma}$, as follows:

$$(1 - D) = (1 - s_t D_c)(1 - s_c D_t) \tag{3}$$

where the scalars s_i $(i = t, c)$ are functions of the stress state $\boldsymbol{\sigma}$:

$$s_i = 1 - w_i r(\boldsymbol{\sigma}) \tag{4}$$

$$r(\boldsymbol{\sigma}) = \sum_{i=1,3} \langle \sigma_i \rangle \Big/ \sum_{i=1,3} |\sigma_i| \qquad \langle \sigma_i \rangle = \frac{1}{2}(\sigma_i + |\sigma_i|) \tag{5}$$

in which σ_i $(\sigma_1 \geq \sigma_2 \geq \sigma_3)$ are the principal stresses of $\boldsymbol{\sigma}$ and the constant $w_i \in [0,1]$ $(i = t, c)$ are responsible for controlling the elastic stiffness recovery, as the principal stresses changes sign. Those constants are assumed to be material properties. For cementitious materials, ABAQUS theory manual [20] recommends $w_t = 0.0$ and $w_c = 1.0$. Finally, from the stress-strain relationship (2), the definition of the effective stress tensor $\overline{\boldsymbol{\sigma}}$, used in the damage-plasticity models, can be established:

$$\overline{\boldsymbol{\sigma}} = \boldsymbol{C}_0 : (\boldsymbol{\varepsilon} - \boldsymbol{\varepsilon}_p) \qquad \overline{\boldsymbol{\sigma}} = \frac{\boldsymbol{\sigma}}{(1 - D)} \tag{6}$$

2.2 Uniaxial behavior under tension and compression

The scalar damages D_t and D_c can be easily defined from uniaxial tensile and compressive tests. The behavior under uniaxial tension and compression of the specific SHCC considered in the present work is described in detail in Santos Júnior et. al. [13]. For illustrative purposes, Figure 2 shows a schematic representation of the uniaxial response of the SHCC under tension and compression.

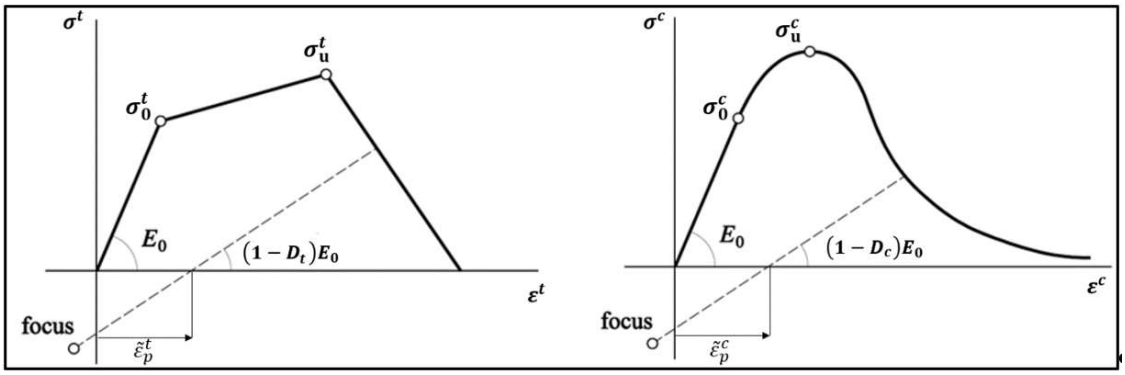

Figure 2. Uniaxial stress-strain behavior: (a) tension; (b) compression

where σ^t, σ^c are the uniaxial engineering stresses and ε^t, ε^c are the engineering uniaxial strains in tension and compression, respectively. σ_0^t and σ_u^t are the first cracking and ultimate tensile stresses, while σ_0^c and σ_u^c are first compression crushing and ultimate compressive stresses. Relating the uniaxial SHCC behavior to uniaxial damage-plasticity models, one writes:

$$\sigma^t = (1-D_t)E_0\left(\varepsilon^t - \tilde{\varepsilon}_p^t\right) \qquad \sigma^c = (1-D_c)E_0\left(\varepsilon^c - \tilde{\varepsilon}_p^c\right) \tag{7}$$

where E_0 is the initial elastic (undamaged) stiffness modulus of the material. D_t and D_c are the tensile and compressive damage scalar variables. Since the uniaxial stiffness degradation is different in the uniaxial tension and in compression tests, the evolution of D_t and D_c is also different. The evolution of D_t and D_c depends on the equivalent plastic strains $\tilde{\varepsilon}_p^t$ and $\tilde{\varepsilon}_p^c$, respectively, and on other field variables, such as the temperature. In the present work, it is assumed that the evolution of these variables depends only on the equivalent plastic strains, i.e., $D_t = D_t\left(\tilde{\varepsilon}_p^t\right)$ and $D_c = D_c\left(\tilde{\varepsilon}_p^c\right)$.

2.3 Damage evolution for brittle materials

The evolution laws for the damage variables D_t and D_c used in this work for brittle materials were obtained based on the work by Birtel and Mark [21]:

$$D_t = 1 - \frac{\frac{\sigma_0^t}{E_0}}{\varepsilon_p^t\left(\frac{1}{b_t}-1\right)+\frac{\sigma_0^t}{E_0}} \qquad D_c = 1 - \frac{\frac{\sigma_0^c}{E_0}}{\varepsilon_p^c\left(\frac{1}{b_c}-1\right)+\frac{\sigma_0^c}{E_0}} \tag{8}$$

in which the constant factors b_t and b_c can be easily obtained from cyclic experimental uniaxial tensile and compressive tests. The values that best fitted Birtel and Mark [21] experimental results were $b_t = 0.1$ and $b_c = 0.7$, which were the ones adopted for the damage evolution in standard concrete models.

2.4 Damage evolution for strain-hardening cementitious materials

For strain-hardening materials, the evolution laws for the damage variables D_t and D_c were obtained based on the work by Santos et al. [13]. To introduce such a law, Figure 3 shows a curve σ_f in the engineering stress-strain space obtained from experimental data of a uniaxial monotonic loading test. Notice that knowing an explicitly integrable expression $\sigma_f = \sigma_f(\varepsilon)$ it is possible to obtain the dissipated strain energy $e_d = W_0 - W_f$ as a function of the total strain

$$e_d(\varepsilon) = W_0 - W_f = D_f \mathrm{W}_0 = \frac{E_0\varepsilon^2}{2} - \int_0^{\varepsilon} \sigma_f(\xi)d\xi \tag{9}$$

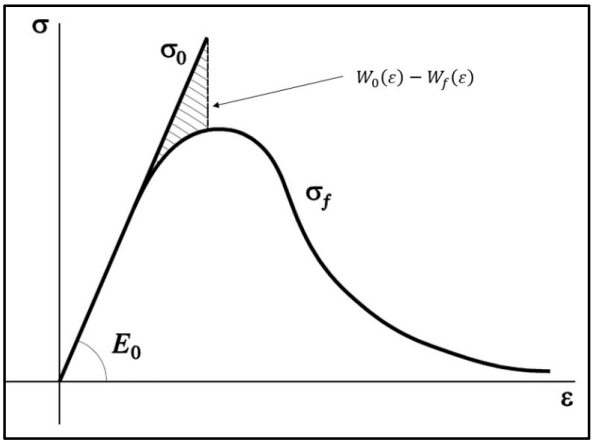

Figure 3. Dissipated energy in uniaxial tests

in which

$$D_f(\varepsilon) = \frac{W_0 - W_f}{W_0} \qquad W_0(\varepsilon) = \int_0^{\varepsilon} \sigma_0(\xi) d\xi = \int_0^{\varepsilon} E_0 \xi d\xi = \frac{E_0 \varepsilon^2}{2} \qquad W_f(\varepsilon) = \int_0^{\varepsilon} \sigma_f(\xi) d\xi \tag{10}$$

are, respectively, the normalized dissipated energy, the strain energy for an undamaged linear elastic material ($D = 0$) and the strain energy for a material with uniaxial stress-strain curve equal to the fitting curve σ_f obtained from an adjustment (minimum squares) of the experimental data. E_0 is the initial tangent modulus of the undamaged material. To account for plastic strains into the damage evolution law, a damage-plasticity uniaxial constitutive model

$$\sigma(\varepsilon) = (1 - D) E_0 \left(\varepsilon - \varepsilon_p\right) \tag{11}$$

must be considered for the computation of the dissipated energy, where D is an irreversible scalar damage variable, which it´s evolution considers the influence of the plastic strains ε_p into the energy dissipation process. Similarly, the recoverable part of energy (or free energy) W_p can be computed, considering now the damage-plasticity model

$$W_p(\varepsilon) = \int_0^{\varepsilon} \sigma(\xi) d\xi = \int_0^{\varepsilon} \left(1 - D(\xi)\right) E_0 \left(\xi - \varepsilon_p(\xi)\right) d\xi \tag{12}$$

$$W_p(\varepsilon) = \frac{E_0 \varepsilon^2}{2} - E_0 \left[\int_0^{\varepsilon} D(\xi) \xi d\xi + \int_0^{\varepsilon} \varepsilon_p(\xi) d\xi - \int_0^{\varepsilon} D(\xi) \varepsilon_p(\xi) d\xi \right]$$

Considering that $W_0 - W_p = e_d(\varepsilon) = W_0 - W_f = D_f W_0$, the damage evolution law $D(\varepsilon)$ can be stablished as:

$$\int_0^{\varepsilon} D(\xi) \xi d\xi + \int_0^{\varepsilon} \varepsilon_p(\xi) d\xi - \int_0^{\varepsilon} D(\xi) \varepsilon_p(\xi) d\xi = D_f(\varepsilon) \frac{\varepsilon^2}{2} \tag{13}$$

$$D(\varepsilon)\varepsilon + \varepsilon_p(\varepsilon) - D(\varepsilon)\varepsilon_p(\varepsilon) = \frac{d}{d\varepsilon} \left[D_f(\varepsilon) \frac{\varepsilon^2}{2} \right]$$

$$D(\varepsilon) = \frac{\frac{d}{d\varepsilon} \left[D_f(\varepsilon) \frac{\varepsilon^2}{2} \right] - \varepsilon_p(\varepsilon)}{\varepsilon - \varepsilon_p(\varepsilon)}$$

In the present study, the plastic strains for SHCC materials were obtained from the focus point concept [23, 24]. The focus in tension and compression for SHCC materials were proposed by Cai et al. [23]. Knowing the focal point coordinates $\mathbf{f} = \{\varepsilon_*, \sigma_*\}^T$ and the fitting curve σ_f, the plastic strain can then be computed as the distance between the intersection of the unload path with the abscissa axis (strain axis) and the origin [13]. Regarding fitting curves σ_f^t and σ_f^c obtainted from the experimental results by Cheng et al. [22] for an SHCC material, the damages evolutions D_t and D_c were obtained to be applied in the structural analysis.

2.5 Concrete plasticity

The yielding surface proposed by Lubliner et. al. [25], which was based on the previous works [26-28], and further modified by Lee and Fenves [16], is controlled by the hardening variables $\tilde{\varepsilon}_p^t$ and $\tilde{\varepsilon}_p^c$, which corresponds to the equivalent tensile and compressive plastic strains, respectively. It is defined in terms of the invariants $\bar{\sigma}_1$, $\bar{p}$ and $\bar{q}$ of the effective stress tensor $\overline{\boldsymbol{\sigma}}$ as:

$$F(\overline{\boldsymbol{\sigma}}) = \frac{1}{1-\alpha}\left(\bar{q} - 3\alpha\bar{p} + \beta\left(\tilde{\boldsymbol{\varepsilon}}_p\right)\langle\bar{\sigma}_1\rangle - \gamma\langle-\bar{\sigma}_1\rangle\right) - \bar{\sigma}^c\left(\tilde{\varepsilon}_p^c\right) = 0 \tag{14}$$

where $\bar{\sigma}_1$ is the maximum principal effective stress, $\bar{p} = -\operatorname{tr}(\overline{\boldsymbol{\sigma}})/3$ is the effective hydrostatic effective pressure and $\bar{q} = \sqrt{2/3\,(\overline{\boldsymbol{S}}:\overline{\boldsymbol{S}})}$ the von Mises effective stress, with $\overline{\boldsymbol{S}} = \overline{\boldsymbol{\sigma}} + \bar{p}\mathbf{I}$ being the deviatory effective stress tensor. In equation (22), $\langle\cdot\rangle$ denotes the positive Macauley bracket The uniaxial tensile and compressive effective stresses: $\bar{\sigma}^t\left(\tilde{\varepsilon}_p^t\right) = \sigma^t\left(\tilde{\varepsilon}_p^t\right)/\left(1 - D_p^t\right)$ and $\bar{\sigma}^c(\tilde{\varepsilon}_p^c) = \sigma^c\left(\tilde{\varepsilon}_p^c\right)/\left(1 - D_p^c\right)$, controlled by the hardening variables $\tilde{\boldsymbol{\varepsilon}}_p = \tilde{\varepsilon}_p^c, \tilde{\varepsilon}_p^t$, defines the hardening parameter:

$$\beta\left(\tilde{\boldsymbol{\varepsilon}}_p\right) = \frac{\bar{\sigma}^c(\tilde{\varepsilon}_p^c)}{\bar{\sigma}^t\left(\tilde{\varepsilon}_p^t\right)}(1-\alpha) - (1+\alpha) \tag{15}$$

where α and γ are positive valued material constants. A non-associated plastic flow rule is assumed with a plastic potential G defined as the hyperbolic Drucker-Prager function:

$$G(\overline{\boldsymbol{\sigma}}) = \sqrt{(\epsilon\sigma_0^t tan\Psi)^2 + \bar{q}^2} - \bar{p}tan\Psi \tag{16}$$

where $\bar{p}$ and $\bar{q}$ are invariants of the effective stress tensor $\overline{\boldsymbol{\sigma}}$, being $\bar{p} = -\bar{I}_1/3$ the effective hydrostatic pressure, and $\bar{q}$ the von Mises effective stress, previous defined. Ψ is the dilation angle, measured in the $\bar{p} \times \bar{q}$ plane, for high values of $\bar{p}$. σ_0^t is the uniaxial tensile stress at the end of the elastic regime and ϵ is an eccentricity parameter, which defines the rate at which the hyperbolic curve $G(\bar{p}, \bar{q}) = 0$ approaches the asymptote straight lines $\|\bar{q}\| = tan\Psi\bar{p}$, which is obtained making $\epsilon = 0$ for the curve $G(\bar{p}, \bar{q}) = 0$.

3 Finite element model results

B. H. Al-Humeidawi and P. Mandal [10] developed an experimental device, illustrated in Figure 4(a), to evaluate the load transfer mechanism between concrete structures by dowel bars, which is a common problem in jointed plain concrete pavements. The analysed structure consisted in two cementitious (standard concrete) blocks and a dowel bar, which could be either made of steel or made of glass fiber reinforced polymer (GFRP). To evaluate the SHCC structural performance, and compare it against the standard concrete performance, the load transfer structure was modelled considering both SHCC and standard concrete materials for the cementitious blocks. Figure 4(b) illustrates the developed finite element models. Regarding the two different cementitious materials and the two different types of dowel bars, four different numerical models were developed: Concrete-Steel model, Concrete-GFRP model, SHCC-Steel model and SHCC-GFRP model. In the following, the validation by comparison of the experimental results with the Concrete-Steel and Concrete-GFRP numerical model results is presented. Later, a comparative study of damage evaluation in the four numerical models will be presented,

showing a potential advantage of the use of alternative materials such as the SHCC and the GFRP for reducing the damage in the vicinity of the dowel bar.

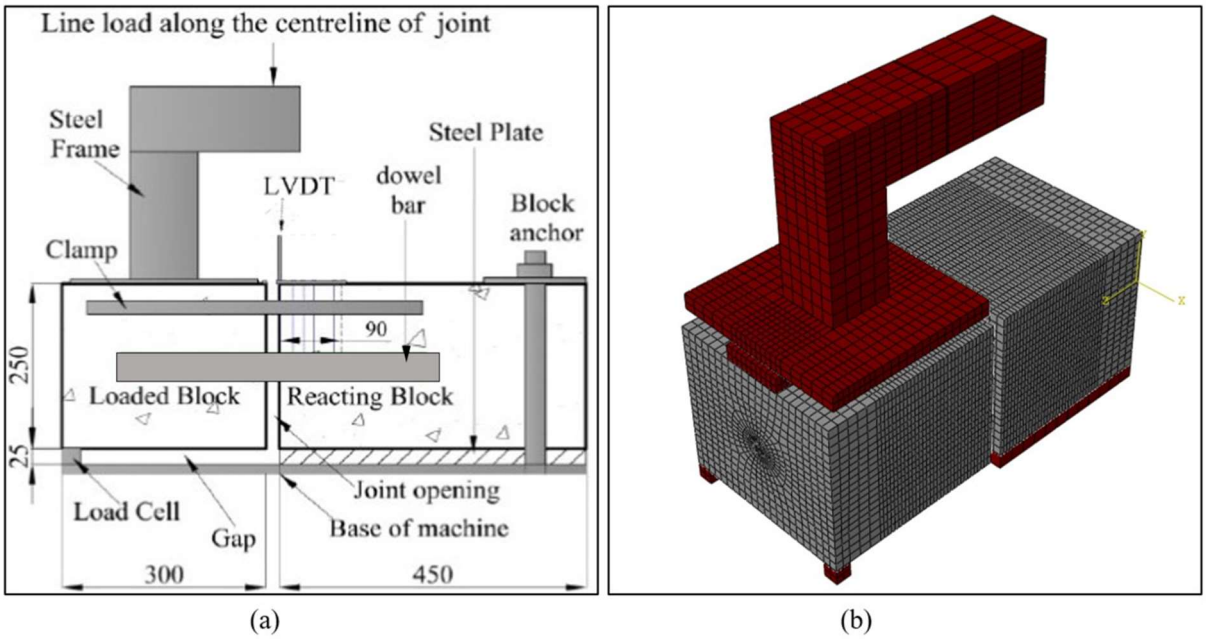

Figure 4. Representative structure: (a) component parts [29]; (b) finite element model

3.1 Validation

The validation of the models was made taking the experimental displacement data of the upper surface of the bar at the face of the reacting block, available in Al-Humeidawi and Mandal [10]. Details of the developed finite element model can be found in Santos Júnior et al. [30]. Figure 5 shows the comparison between the experimental results and the ones obtained from the developed numerical models. A very good agreement is observed between the experimental and numerical results. Thus, it´s possible to ensure that the boundary and contact conditions of the model were adequate to reproduce the experimental test proposed by Al-Humeidawi and Mandal [10]. In the following, the same model will be studied, regarding now the SHCC material discussed in Santos Júnior et al. [13]. A comparative study of damage distribution near the bar regarding both SHCC and standard concrete will be presented.

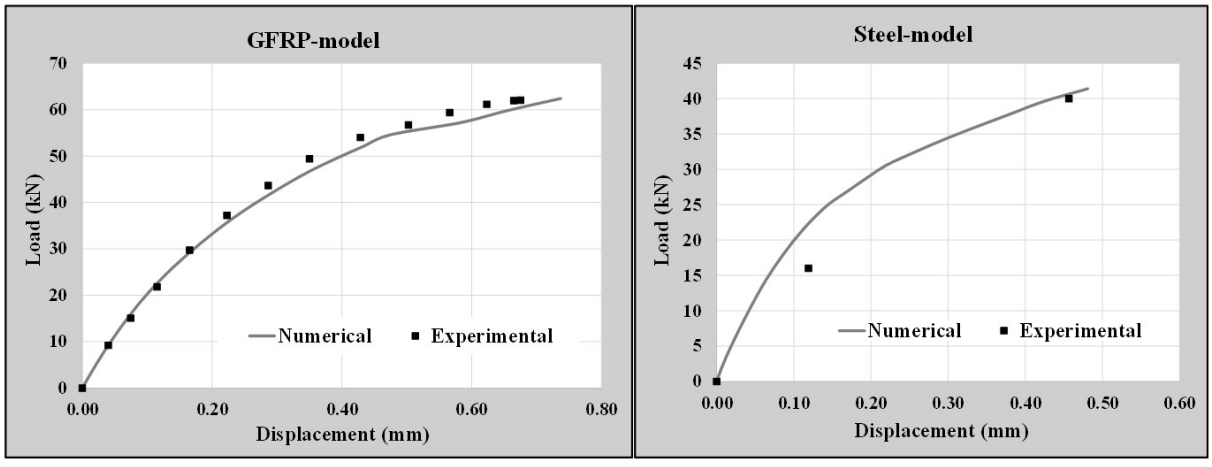

Figure 5. Experimental and numerical results: (a) GFRP bar model; (b) Steel bar model

3.2 Damage evaluation: Standard concrete versus SHCC

After the model updating, it is possible to perform a comparative evaluation of damage near the dowel bar, regarding both standard concrete and the SHCC blocks, by simply changing the constitutive model of the cementitious material. However, the standard concrete studied by Al-Humeidawi and Mandal [10] has a modulus $E_0 = 28$ GPa, while the SHCC mixture developed by Cheng et al. [22] and discussed in Santos Júnior et al. [13] has a modulus $E_0 = 20$ GPa. Thus, the straightforward compassion may be unfair, since the standard concrete has a higher stiffness and, thus, it is expected to be more damaged after the loading. To be able to perform a fair comparison, the standard concrete was modelled with the CDP model, adjusted to represent the C12 standard concrete presented in the CEB-FIB Model Code 1990 [31], which has a modulus of $E_0 = 22.9$ GPa, the closest one to the SHCC mixture under consideration. The stress-strain curves in uniaxial compression of such concrete were obtained following the CEB-FIB Model Code 2010 [32] instructions. From these curves, the damage evolutions in compression and tension were obtained, following the model by Birtel and Mark [21]. The SHCC material parameters used in the CDP constitutive model for the simulations were the same discussed in Santos Júnior et al. [13].

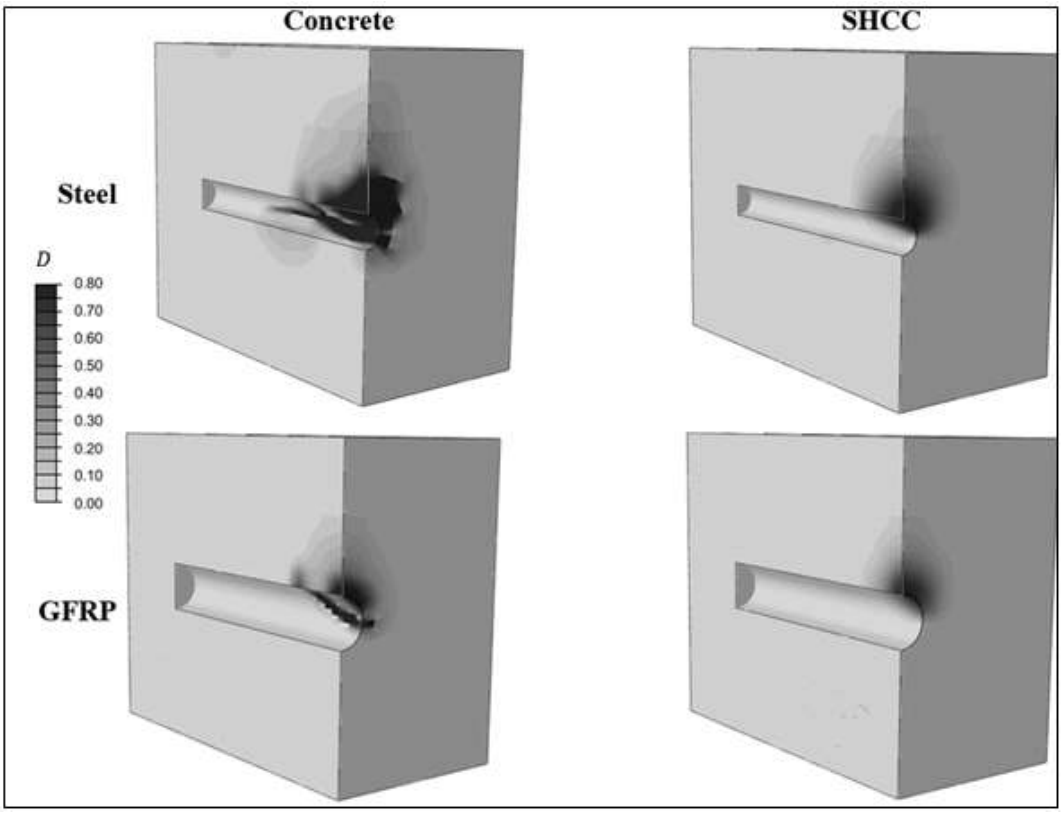

Figure 6. Scalar damage field for the loaded block

A qualitative damage evaluation for both loaded and reaction blocks (see Figure 4a) was performed based on the numerical field of the scalar isotropic damage variable D, discussed in Section 2.1. Figures 6 and 7 presents the visualization of the damage variable for the loaded and reaction blocks, respectively. These results are presented for the load level of 37 kN, which corresponds to the ultimate load for the most restrictive model, C12 concrete and steel bar. The analysis of the damage results allows to observe a significant damage reduction in both blocks regarding the adoption of SHCC materials instead of standard concrete. Besides, there is also a considerable reduction due to the adoption of GFRP bars instead of the traditional steel ones, pointing out that the adoption of such alternative materials may help to improve the structural life of join plain concrete pavement structures.

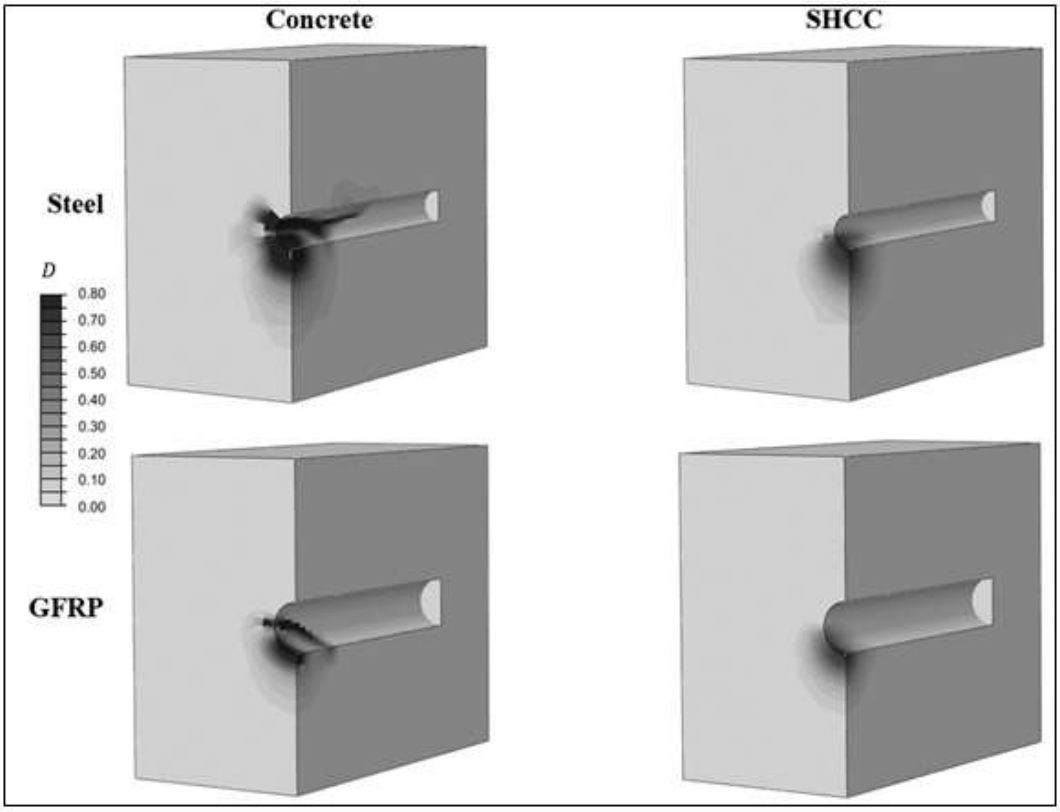

Figure 7. Scalar damage field for the reaction block

4 Conclusions

This paper evaluated numerically the differences in the damage distribution in the cementitious material near the dowel bars in JPCP considering both standard concrete and SHCC and alternative materials for the dowel bars. A finite element model was developed using Abaqus and validated from the available experimental results. The evolution law of the scalar damage variables, as well as the other material parameters for the CDP constitutive model, were updated to reproduce standard concrete and SHCC structural responses. Regarding the SHCC model, an adequate evolution law to be applied in strain-hardening damageable materials developed by the authors in a previous work [13] was utilized. Two different materials were analyzed for the dowel bar: steel and GFRP, a transversely isotropic material, alternative to steel. The damage near the bar was quantified and compared regarding both standard concrete and SHCC blocks. Advantages regarding the use of alternative materials, such as the SHCC and polymeric bars, instead of standard concrete and steel bars, were highlighted in the application.

Authorship statement. The authors hereby confirm that they are the sole liable persons responsible for the authorship of this work, and that all material that has been herein included as part of the present paper is either the property (and authorship) of the authors or has the permission of the owners to be included here.

References

[1] E. J. Yoder and M. W. Witczak. *Principles of pavement design*. John Wiley & Sons, 1991.
[2] Y. H. Huang. *Pavement analysis and design*. Prentice-Hall, 1993.
[3] P. Mackiewicz. "Finite-element analysis of stress concentration around dowel bars in jointed plain concrete pavement". *Journal of Transportation Engineering*, vol. 141, n. 6, pp. 06015001 (1–8), 2015.

[4] A. Wadkar, Y. Metha, D. Cleary, A. Zapata, L. Musumeci and K. William. "Effect of aircraft gear positions and gear configurations on load transfer efficiency of airfield rigid pavement joints". *Road Pavement and Material Characterization, Modeling, and Maintenance*. pp. 40–48, 2011.
[5] J. Kim and K. D. Hjelmstad. "Three-dimensional finite element analysis of doweled joints for airport pavements". *Transportation Research Record*, vol. 1853, n. 1, pp. 100–109, 2003.
[6] V. Sadeghi and S. Hesami. "Investigation of load transfer efficiency in jointed plain concrete pavements (JPCP) using FEM". *International Journal of Pavement Research and Technology*, vol. 11, n. 3, pp. 245–252, 2018.
[7] S. N. Shoukry, G. W. William, M. Y. Riad and S. V. S. Motamarri. Effect of Bonding Force on Stresses in Concrete Slabs. PhD thesis, West Virginia University, College of Engineering and Mineral Resources, 2003.
[8] M. Prabhu, A. Varma and N. Buch. "Analytical investigation of the effects of dowel misalignment on concrete pavement joint opening behaviour". *International Journal of Pavement Engineering*, vol. 10, n. 1, pp. 49–62, 2009.
[9] B. H. Al-Humeidawi and P. Mandal. "Experimental investigation on the combined effect of dowel misalignment and cyclic wheel loading on dowel bar performance in JPCP". *Engineering Structures*, vol. 174, pp. 256–266, 2018.
[10] B. H. Al-Humeidawi and P. Mandal. "Evaluation of performance and design of GFRP dowels in jointed plain concrete pavement–part 1: experimental investigation". *International Journal of Pavement Engineering*, vol. 15, n. 5, pp. 449–459, 2014.
[11] V. C., Li. *Engineered Cementitious Composites (ECC): Bendable Concrete for Sustainable and Resilient Infrastructure*. Springer, 2019.
[12] A. G. Benjamin. "Material Property Characterization of Ultra-High Performance Concrete". FHWA-HRT-06-103, p. 186, 2006.
[13] E. J. Santos Júnior, P.A. Krahl, F.A.C. Monteiro, S.G.F. Cordeiro. "New damage evolution law for modelling Strain-Hardening Fiber-Reinforced Cementitious Composites". Materials & Structures, Submitted, 2022.
[14] E. J. Santos Júnior. A damage evolution law for the constitutive modeling of SHCC materials: Application to load transfer in pavements. Master thesis. Aeronautics Institute of Technology (Brazil), 2022.
[15] J. Lubliner, J. Oliver, S. Oller and E. Onate. "A plastic-damage model for concrete". *International Journal of solids and structures*, vol. 25, n. 3, pp. 299–326, 1989.
[16] J. Lee and G. L. Fenves. "Plastic-damage model for cyclic loading of concrete structures". *Journal of engineering mechanics*, vol. 124, n. 8, pp. 892–900, 1998.
[17] Y. Tao and J. Chen. "Concrete damage plasticity model for modeling FRP-to-concrete bond behavior". *Journal of composites for construction*, vol. 19, n. 1, pp. 04014026 (1–13), 2015.
[18] H. Othman and H. Marzouk. "Finite-element analysis of reinforced concrete plates subjected to repeated impact loads". *Journal of Structural Engineering*, vol. 143, n. 9, pp. 04017120 (1–16), 2017.
[19] N. F. Hany, E. G. Hantouche and M. H. Harajli. "Finite element modeling of FRP-confined concrete using modified concrete damaged plasticity". *Engineering Structures*, vol. 125, pp. 1–14, 2016.
[20] ABAQUS, Theory Manual, Hibbitt, Karlsson & Sorensen Inc., 2013.
[21] V. Birtel and P. Mark. Parameterized finite element modelling of RC beam shear failure. In: ABAQUS users' conference. 2006.
[22] H. Cheng, C.M. Paz, B.C. Pinheiro and S.F. Stefen. "Experimentally based parameters applied to concrete damage plasticity model for strain hardening cementitious composite in sandwich pipes." *Materials and Structures*, vol. 53, n. 4, pp. (1–17), 2020.
[23] J. Cai, J. Pan, J. Tan and B. Vandevyvere. "Nonlinear finite-element analysis for hysteretic behavior of ECC-encased CFST columns.".*Structures*, vol. 25, pp. (670–682), 2020.
[24] D.Z. Yankelevsky, H.W. Reinhardt. "Model for cyclic compressive behavior of concrete."*Journal of Structural Engineering*, vol. 113, pp. (228–240), 1987.
[25] J. Lubliner, J. Oliver, S. Oller and E. Onate. "A plastic-damage model for concrete". *International Journal of solids and structures*, vol. 25, n. 3, pp. 299–326, 1989.
[26] A.C. Chen and W.F. Chen. "Constitutive relation for concrete". Journal of the Engineering Mechanics Division, vol. 101, n. 4, pp. 465–481, 1975.
[27] N.S. Ottosen. "A failure criterion for concrete". Journal of the Engineering Mechanics Division, vol. 103, n. 4, pp. 527–535, 1977.
[28] J. Podgórski. "General failure criterion for isotropic media". Journal of Engineering Mechanics, vol. 111, n. 2, pp. 188–201, 1985.
[29] B. Al-Humeidawi. Evaluation of the performance of GFRP dowels in jointed plain concrete pavement)JPCP) for road/airport under the combined effect of dowel misalignment and cyclic wheel load. Ph.D thesis. The University of Manchester (United Kingdom), 2013.
[30] E.J. Santos Júnior, S.G.F. Cordeiro, F.A.C. Monteiro. "A numerical study of damage evaluation in jointed plain concrete pavements considering alternative materials for dowel bars". In XLII Ibero-Latin-American Congress on Computational Methods in Engineering, CILAMCE, 2021.
[31] COMITÉ EURO-INTERNATIONAL DU BÉTON. CEB-FIB Model Code 1990. Thomas Telford Services, Ltd., London, 1993.
[32] COMITÉ EURO-INTERNATIONAL DU BÉTON. CEB-FIB Model Code 2010. First complete draft, Lausanne, Switzerland, 2010.